Research in Astron. Astrophys. **2012** Vol. **12** No. **1**, 104–114
http://www.raa-journal.org *http://www.iop.org/journals/raa*

Research in Astronomy and Astrophysics

Kinematics and amplitude evolution of global coronal extreme ultraviolet waves *

Ting Li[1], Jun Zhang[1], Shu-Hong Yang[1] and Wei Liu[2,3]

[1] Key Laboratory of Solar Activity, National Astronomical Observatories, Chinese Academy of Sciences, Beijing 100012, China; *liting@nao.cas.cn*
[2] Lockheed Martin Solar and Astrophysics Laboratory, Department ADBS, Building 252, 3251 Hanover Street, Palo Alto, CA 94304, USA
[3] W. W. Hansen Experimental Physics Laboratory, Stanford University, Stanford, CA 94305, USA

Received 2011 April 29; accepted 2011 September 22

Abstract With the observations of the Solar-Terrestrial Relations Observatory (*STEREO*) and the Solar Dynamics Observatory (*SDO*), we analyze in detail the kinematics of global coronal waves together with their intensity amplitudes (so-called "perturbation profiles"). We use a semi-automatic method to investigate the perturbation profiles of coronal waves. The location and amplitude of the coronal waves are calculated over a 30° sector on the sphere, where the wave signal is strongest. The position with the strongest perturbation at each time is considered as the location of the wave front. In all four events, the wave velocities vary with time for most of their lifetime, up to 15 min, while in the event observed by the Atmospheric Imaging Assembly there is an additional early phase with a much higher velocity. The velocity varies greatly between different waves from 216 to 440 km s^{-1}. The velocity of the two waves initially increases, subsequently decreases, and then increases again. Two other waves show a deceleration followed by an acceleration. Three categories of amplitude evolution of global coronal waves are found for the four events. The first is that the amplitude only shows a decrease. The second is that the amplitude initially increases and then decreases, and the third is that the amplitude shows an orderly increase, a decrease, an increase again and then a decrease. All the extreme ultraviolet waves show a decrease in amplitude while propagating farther away, probably because the driver of the global coronal wave (coronal mass ejection) is moving farther away from the solar surface.

Key words: Sun: corona — Sun: coronal mass ejections (CMEs) — Sun: flares

1 INTRODUCTION

Observations of large-scale coronal disturbances were first made by the Solar and Heliospheric Observatory (*SOHO*) Extreme Ultraviolet Imaging Telescope (EIT; Thompson et al. 1998) and hence the disturbances were named "EIT waves." These waves were originally thought to be the coronal

* Supported by the National Natural Science Foundation of China.

counterparts of the chromospheric Moreton waves (Moreton & Ramsey 1960), interpreted as the "skirt" of a coronal fast-mode magnetoacoustic shock wave (Uchida 1968).

Afterwards, it was assumed that global coronal waves were different from Moreton waves in many aspects. Global coronal waves have broad circular fronts, but Moreton waves are generally narrower than semicircles. The velocities of global coronal waves ($\sim$170$-$350 km s^{-1}) are on average smaller than Moreton waves ($\sim$1 000 km s^{-1}) (Smith & Harvey 1971; Klassen et al. 2000). Moreover, global coronal waves occur much more frequently than Moreton waves. Chen et al. (2005) and Chen (2008, 2009) suggested that the sharp extreme ultraviolet (EUV) front is the real coronal counterpart of the Moreton wave, and is different from the diffuse global coronal wave. According to the model of Chen et al. (2005), there should be two kinds of waves associated with a strong coronal mass ejection (CME): one is the fast-mode shock wave and the other is the slower global coronal wave.

There were two main debates after the discovery of global coronal waves. One is whether global coronal waves are real waves (Wang 2000; Warmuth et al. 2001; Wills-Davey et al. 2007; Patsourakos & Vourlidas 2009) or rather propagating disturbances related to the magnetic field line opening and restructuring associated with CME expansion (Delannée 2000; Chen et al. 2002; Attrill et al. 2007a,b; Chen 2006; Chen & Zong 2009; Li et al. 2010, 2011). Zhukov & Auchère (2004) and Cohen et al. (2009) suggested that the global coronal wave was a combination of both true wave and non-wave mechanisms. Another debate is about whether global coronal waves are initiated by the erupting CME or the explosive flare energy release. Recently, statistical studies (Biesecker et al. 2002; Cliver et al. 2005; Chen 2006; Patsourakos et al. 2009) showed global coronal waves to be more closely associated with CMEs than with flares. Moreover, global coronal waves were found to stop near coronal hole boundaries by Thompson & Myers (2009). Later, Gopalswamy et al. (2009) found that the EIT waves on 2007 May 19 were reflected at coronal hole boundaries, for which Attrill (2010) had a different interpretation. For recent reviews, we refer to Vršnak & Cliver (2008), Wills-Davey & Attrill (2009) and Gallagher & Long (2011).

One important drawback of coronal wave studies is the limitations of the *SOHO*/EIT (Delaboudinière et al. 1995) observations. The low cadence of the EIT instrument (12$-$15 min) causes significant confusion about the propagating characteristics of global coronal waves. Since the launch of the Solar-Terrestrial Relations Observatory (*STEREO*; Kaiser et al. 2008) and the Solar Dynamics Observatory (*SDO*; Schwer et al. 2002), the high-cadence observations in different EUV passbands have been used to investigate the kinematic and amplitude evolution of propagating coronal waves.

The kinematics of global coronal waves has been studied for over a decade. However, there have been no consistent results so far. Recently, Kienreich et al. (2009) found that the wave propagates globally over the whole disk with a constant velocity of 236$\pm$16 km s^{-1}. Ma et al. (2009) also found constant velocities in global EUV wave propagation using *STEREO* observations. However, Warmuth et al. (2004) studied 12 flare-associated wave events using Hα, EUV, He I 10830 Å, SXR and radioheliographic data. They found that the waves in all the events were decelerating, which explains the apparent "velocity discrepancy" between Moreton and global coronal waves. Veronig et al. (2008) concluded that the coronal wave reveals deceleration, indicative of a freely propagating magnetohydrodynamic (MHD) wave. For the same event, Long et al. (2008) observed that the wave accelerated at first and then decelerated when it was far from the source region.

In this paper, we study four events observed by the *STEREO* and *SDO*, and analyze in detail the kinematics of global coronal waves together with their intensity amplitudes (so-called "perturbation profiles"). Section 2 describes the observations and sampling criteria for these events. In Section 3 we sample these four coronal waves by examining their propagation characteristics, and the conclusions and discussion are presented in Section 4.

2 OBSERVATIONS

The twin spacecrafts of the *STEREO* mission have already provided a rich database since their launch in 2006 October, with images both in visible and EUV lines. The Sun Earth Connection Coronal and Heliospheric Investigation (SECCHI; Howard et al. 2008) imaging package on each spacecraft consists of the following five telescopes: the Extreme Ultraviolet Imager (EUVI; see Wuelser et al. 2004), inner (COR1) and outer (COR2) coronagraphs, and inner (HI1) and outer (HI2) heliospheric imagers. EUVI images are taken at four wavelengths centered at 304, 171, 195 and 284 Å with time cadences of 10, 2.5, 10 and 20 min, respectively. COR1 has a field of view (FOV) from 1.4 to 4 $R_\odot$ and the FOV of COR2 is from 2.5 to 15 $R_\odot$.

Images from the Atmospheric Imaging Assembly (AIA; Lemen et al. 2011) on the *SDO* are taken in 10 different wavelength bands, including one visible line, two ultraviolet and seven EUV channels. It provides full-disk images, covering a wide range of temperatures, with high cadence (up to 12−24 s) and spatial resolution ($0.6''$ pixel^{-1}).

We examined 171 and 195 Å data observed by EUVI from 2007 January to 2009 December and selected three coronal wave events. The sampling criteria for these events are summarized as follows:

(1) The source region of the event is within 50° of the visible Sun center.
(2) Either the 171 or 195 Å images, or both, have a time cadence of at least 2.5 min.
(3) The wave fronts can be well defined in at least four images.

In addition, we investigated a global coronal wave on 2010 June 12 observed by *SDO*/AIA with a high time cadence of 12 s. We concentrated on the 193 Å data to analyze the kinematics and amplitude of the wave because of the strong wave fronts at this wavelength. The data sets used in this study are summarized in Table 1, introducing the four events indexed 1 to 4.

Table 1 Characteristics of the Sampled Events

No.	Date	GOES	Satellite/Wavelength (Å)	Cadence (min)	Mean Velocity (km s^{-1})
1	2007 Dec 07	B1.4	EUVI-A/171	2.5	276
2	2008 Apr 26	B3.8	EUVI-B/171	2.5	216
3	2007 May 19	B9.5	EUVI-A/171	2.5	431
4	2010 Jun 12	M2.0	AIA/193	0.2	440

The top panels in Figure 1 present a selection of wave images on 2007 December 07 from *STEREO A*. Due to the broad nature of the diffuse bright fronts, we avoid visually determining the wave fronts and use a semi-automatic method (see Podladchikova & Berghmans 2005; Liu et al. 2010; Wills-Davey 2006). We identify the flare kernel as the new "north pole," and draw a 30° wide heliographic "longitude" sector (indicated in the top panels of Fig. 1). The location and amplitude of the coronal wave are calculated over the sector on the sphere, where the wave signal is strongest. We obtain the image profile as a function of distance measured from the flare kernel along the "longitudinal" great circle (thus correcting for the atmosphere's sphericity) by averaging pixels in the "latitudinal" direction.

Figure 2 shows the perturbation profiles of the wave on 2007 December 07, obtained from base difference images. The base image is at 04:26 UT for this wave. All the images are de-rotated to the time of the base image. Each perturbation profile is normalized by the maximum intensity difference, and the difference smaller than zero is set to zero. Thus the data points in Figure 2 are between zero and one. The position with the strongest perturbation at each time is considered as the location of the wave front (dashed lines in Fig. 2). If the location with the largest intensity corresponds to the stationary brightenings, the location with adjacent peak intensity is considered as the position of the

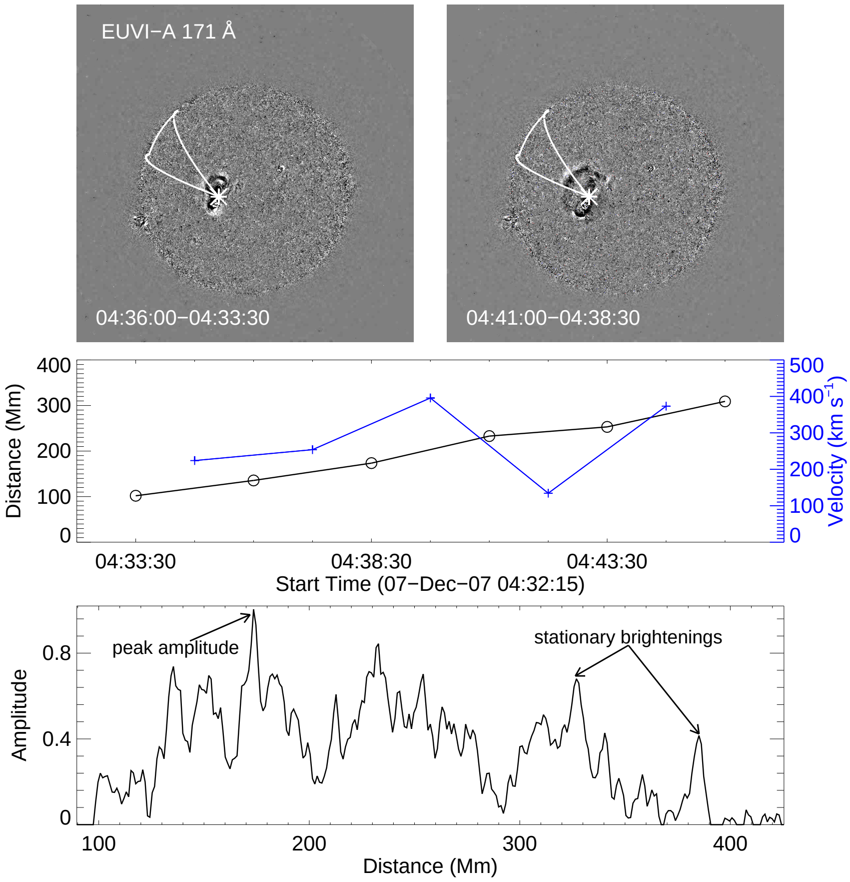

Fig. 1 *Top*: running difference images of the global coronal wave on 2007 December 07. The white curves outline the 30° sector in which the perturbation profiles are calculated, starting from the determined wave center (indicated by the asterisks). *Middle*: distance-time and velocity-time plots of the wave obtained from the base difference profiles (Fig. 2). *Bottom*: amplitude-distance plot of the wave obtained from the base difference profiles (Fig. 2).

coronal wave. Using the locations of the wave fronts, we calculate the distance-time plot (middle panel in Fig. 1). The central difference scheme of two location points is used to derive the velocity. For a certain distance, the amplitude is the maximum intensity among all times. The amplitude-distance plot (bottom panel in Fig. 1) is obtained from Figure 2 in this way.

3 DATA ANALYSIS AND RESULTS

3.1 2007 December 07 (event 1)

On 2007 December 07, a coronal wave occurred in active region (AR) 10977 accompanied by a GOES class B1.4 flare (top panels in Fig. 1). The flare (located at S4°, E14° from the *STEREO A* view) began at 04:35 UT, peaked at 04:41 UT and ended at 04:55 UT. The *STEREO* spacecrafts were separated by 42.4° and both observed the wave. Due to the high spatial resolution of *STEREO A* and high time cadence in 171 Å, we use observations from *STEREO A* in 171 Å to investigate the

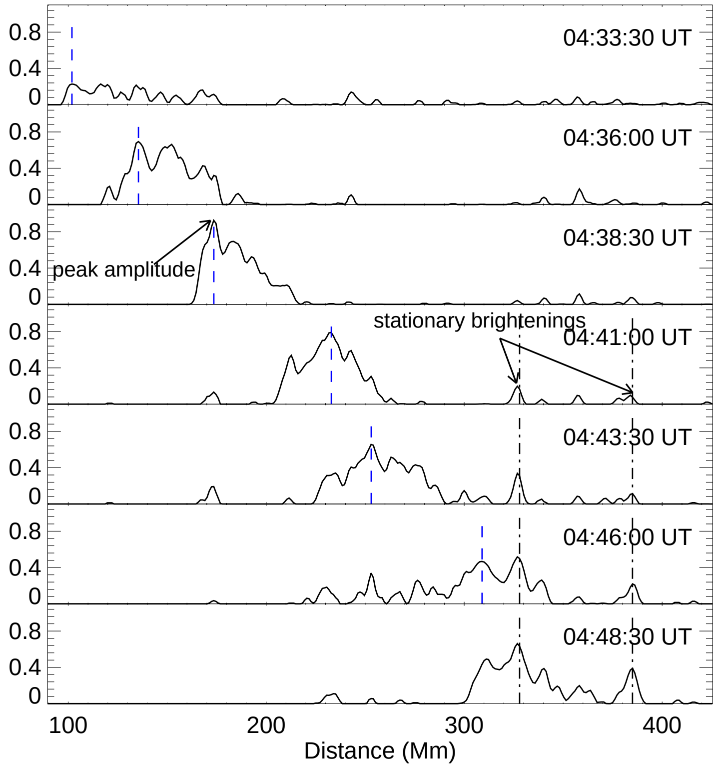

Fig. 2 Perturbation profiles of the wave on 2007 December 07 obtained from 171 Å base difference images. The dashed lines denote the locations of the wave at different times. The dash-dotted lines denote the locations of stationary brightenings.

kinematics and amplitude evolution of the wave. The wave mainly propagated to the northeast after 04:41 UT, and thus we chose a 30° sector in the northeast of the flare kernel (top panels in Fig. 1), where the wave signal is strongest.

By using the semi-automatic method (Liu et al. 2010), we obtain the perturbation profiles of the coronal wave (Fig. 2). Figure 2 presents the base difference profiles during ∼04:33−04:48 UT. The propagation of the coronal wave is well illustrated by the base difference profiles in Figure 2. The distance-time plot of the wave (middle panel in Fig. 1) is obtained from Figure 2. At 04:33 UT, the wave had an initial distance of 102 Mm from the source region. About 15 min later, the wave propagated a distance of 373 Mm. Then the velocities of the wave are calculated according to the distance-time plot (middle panel in Fig. 1). The initial velocity was 224 km s^{-1}, then it increased to 396 km s^{-1} about 5 min later. Afterwards, the wave decelerated to 134 km s^{-1} at 04:42 UT, then it accelerated again and increased to 373 km s^{-1}.

We also use base difference profiles (Fig. 2) to get the perturbation amplitude, since base difference images can show the real perturbation above the initial background value. Seen from Figure 2, the amplitude (profile peak) increased in the initial 5 min, and then decreased afterwards. The humps from the diffuse pulses were regular between 04:36 and 04:43 UT, and then became widely dispersed after 04:46 UT. There were stationary brightenings at distances of 328 and 385 Mm, which were probably caused by magnetic structures. The amplitude-distance plot (bottom panel in Fig. 1) shows that the amplitude of the diffuse pulse increases with distance between 98 and 174 Mm, and subsequently decays with distance.

3.2 2008 April 26 (event 2)

The global coronal wave on 2008 April 26 was observed during ∼13:56−14:16 UT, originating from AR 10989 (top panels in Fig. 3). The event occurred along with a GOES class B3.8 flare located at N15°, W16° (*STEREO B* view), which started at 13:54 UT and ended at 14:38 UT. The event could be observed from both *STEREO* satellites (*STEREO A* and *STEREO B*) which were separated by 49.5°. As seen from *STEREO A*, the wave propagated to the far side of the Sun after 14:01 UT. The EUVI imaging cadence was 2.5 min in the 171 Å filter and 10 min in the 195 Å one. Therefore, we use 171 Å data from *STEREO B* to investigate the kinematics and amplitude evolution of the wave. The wave mainly propagated to the east after 13:59 UT, and thus we chose a 30° sector in the east of the flare kernel (top panels in Fig. 3), where the wave signal is strongest.

We use the same method as event 1 to obtain distance-time and amplitude-distance plots (middle and bottom panels in Fig. 3). At 13:56 UT, the wave was located at a distance of 190 Mm from the source region. About 12 min later, the wave propagated to a distance of 352 Mm. The wave had an

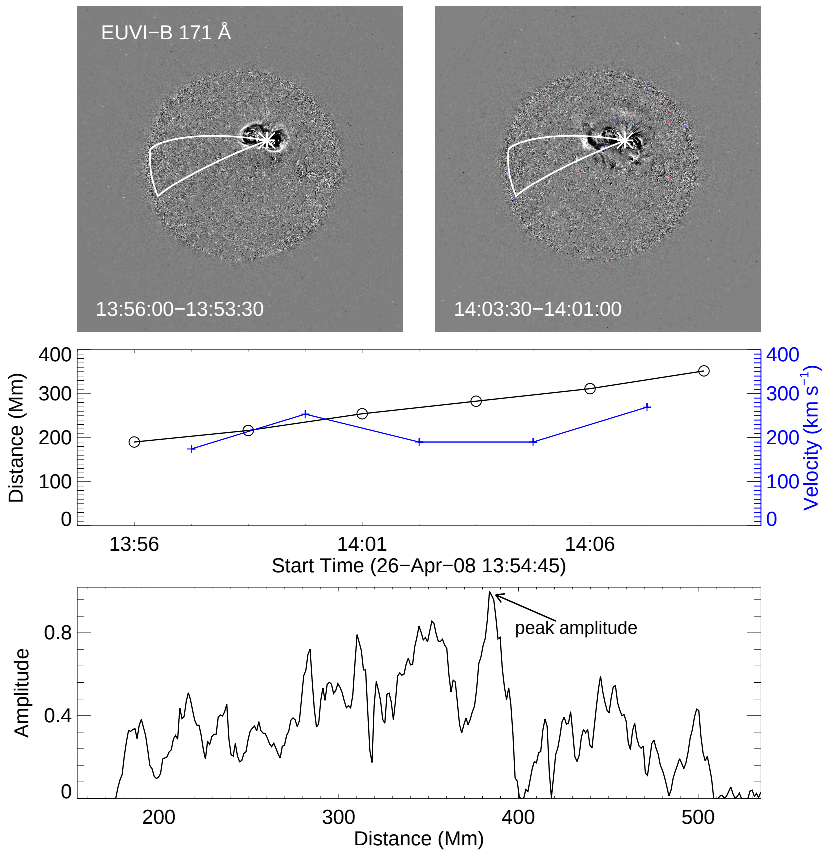

Fig. 3 Similar to Figure 1 but for the global coronal wave on 2008 April 26.

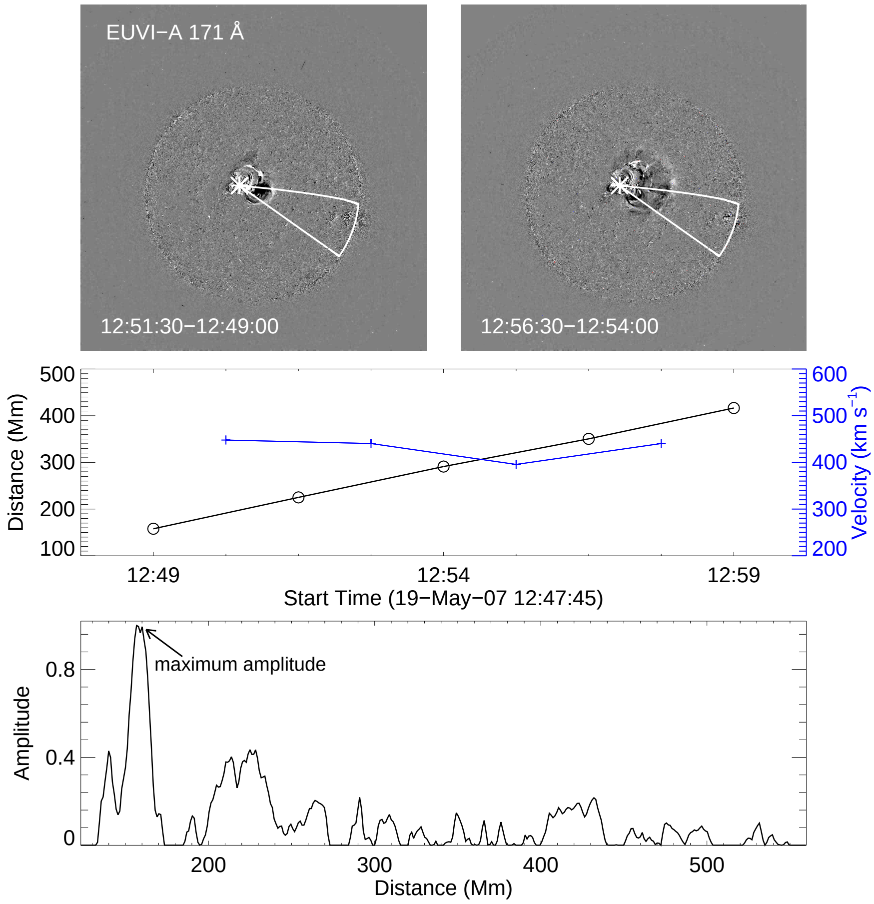

Fig. 4 Similar to Figure 1 but for the global coronal wave on 2007 May 19.

initial velocity of 174 km s^{-1}, and increased to 253 km s^{-1} about 2 min later. Then the velocity decreased to 190 km s^{-1} at 14:05 UT, and subsequently increased to 269 km s^{-1}. As seen from the amplitude-distance plot (bottom panel in Fig. 3), the perturbation amplitude reached its maximum ∼12 min after the onset of the wave, and the corresponding distance was 386 Mm. Then the diffuse pulse showed a decreasing intensity with propagation. The amplitude evolution of this wave was similar to that of event 1.

3.3 2007 May 19 (event 3)

The wave on 2007 May 19 was observed during ∼12:49−13:01 UT, in association with a weak flare (GOES B9.5) in AR 10956 (top panels in Fig. 4). The flare was located at N15°, E7° (*STEREO A* view) and started at 12:34 UT with a maximum at 13:02 UT. The twin STEREO spacecrafts were 8.6° apart and both observed the wave. The EUVI imaging cadence was 2.5 min in the 171 Å filter and 10 min in the 195 Å one. The spatial resolution of *STEREO A* is higher than that of *STEREO B*, and thus we use observations from *STEREO A* in 171 Å.

The expansion towards the southeast is rather weak because there is a coronal hole in the southeast of the AR. The first wave front in 171 Å was obvious at 12:49 UT with an initial distance of

158 Mm from the source region. Then the intensity of the diffuse pulse started to obviously decrease (bottom panel in Fig. 4). The amplitude-distance plot only shows a decrease, which is different from that of events 1 and 2. At 12:59 UT, the wave propagated to a distance of 416 Mm. The initial velocity was 448 km s^{-1} and then decreased to 396 km s^{-1} about 5 min later. Afterwards, the wave accelerated to 440 km s^{-1} at 12:58 UT.

3.4 2010 June 12 (event 4)

The wave on 2010 June 12 was observed by *SDO*/AIA with a time cadence of 12 s (top panels in Fig. 5). The above three events were observed by *STEREO* with a cadence of 2.5 min in 171 or 195 Å. Although the *SDO* observations cover a wide range of temperatures, with high cadence (up to 12s) and spatial resolution ($0.6''$ pixel^{-1}), we concentrate on 193 Å data due to the strong wave fronts at this wavelength. The wave originated from AR 11081, in association with a strong GOES class M2.0 flare (located at N24°, W46° from the SDO view).

The kinematics and amplitude of the wave are calculated over a 30° sector on the sphere (indicated in the top panels). We use 1 min base difference images to obtain the amplitude evolution since they have larger amplitudes than the 12 s images. The base image is at 00:58 UT for this wave. As seen from the amplitude-distance plot (bottom right panel in Fig. 5), the intensity of the wave increases until it propagates to a distance of 314 Mm. Then it increases again at a distance of 412 Mm, and subsequently decreases to nearly zero.

By using 12 s base ratio images, we obtain the stack plot of the global coronal wave (bottom left panel in Fig. 5). As seen from the stack plot, the wave propagated at a larger velocity before ∼01:05 UT. The mean velocity of the leading edge was 770 km s^{-1}. Then the wave decelerated to 330 km s^{-1} in the late stage. We also extract the position of maximum intensity and obtain the distance-time and velocity-time plots in Figure 5. The initial velocity was 748 km s^{-1}, and then it decreased rapidly to 296 km s^{-1} at 01:09 UT. Afterwards, it increased to 322 km s^{-1} about 4 min later.

4 CONCLUSIONS AND DISCUSSION

Using a semi-automatic method, we studied the propagation characteristics of four global coronal waves and found that the velocities of all the waves varied with time. In Table 1, we summarize the results of the four events studied. The mean velocity varies greatly between different waves from 216 to 440 km s^{-1}. The amplitudes of three waves first increase, and then decrease. The amplitude increase lasts 3–12 min. The wave on 2007 May 19 only shows an amplitude decrease after its onset.

Three categories of amplitude evolution of global coronal waves are reported in this work. The first is that the amplitude initially increases and then decreases. The second is that the amplitude only shows a decrease. The third is that the amplitude shows an increase, a decrease, an increase again and then a decrease. Our conclusion is consistent with that made by Muhr et al. (2011). They found that the maximum intensity values of three waves revealed initial intensification and decayed to original levels within 40–60 min. However, the wave on 2007 May 19 only shows a decrease of peak amplitude intensity. Veronig et al. (2010) showed that the wave profile was first steepening and the amplitude was growing. Subsequently, the amplitude was decreasing steadily and the wave profile width was increasing. They suggested that the wave was first driven by CME lateral expansion, and then propagating freely after the end of the driven phase. Furthermore, base difference images are used to get the perturbation on top of the initial background value, and the image before the wave onset is selected as the base image. We examine the amplitude evolution by selecting different base images, and find that the result is not affected by the selected base image.

The kinematics of EIT waves has been studied for a decade, however, no consistent results have been deduced so far. Many authors suggested the constant velocity result (Kienreich et al. 2009; Ma

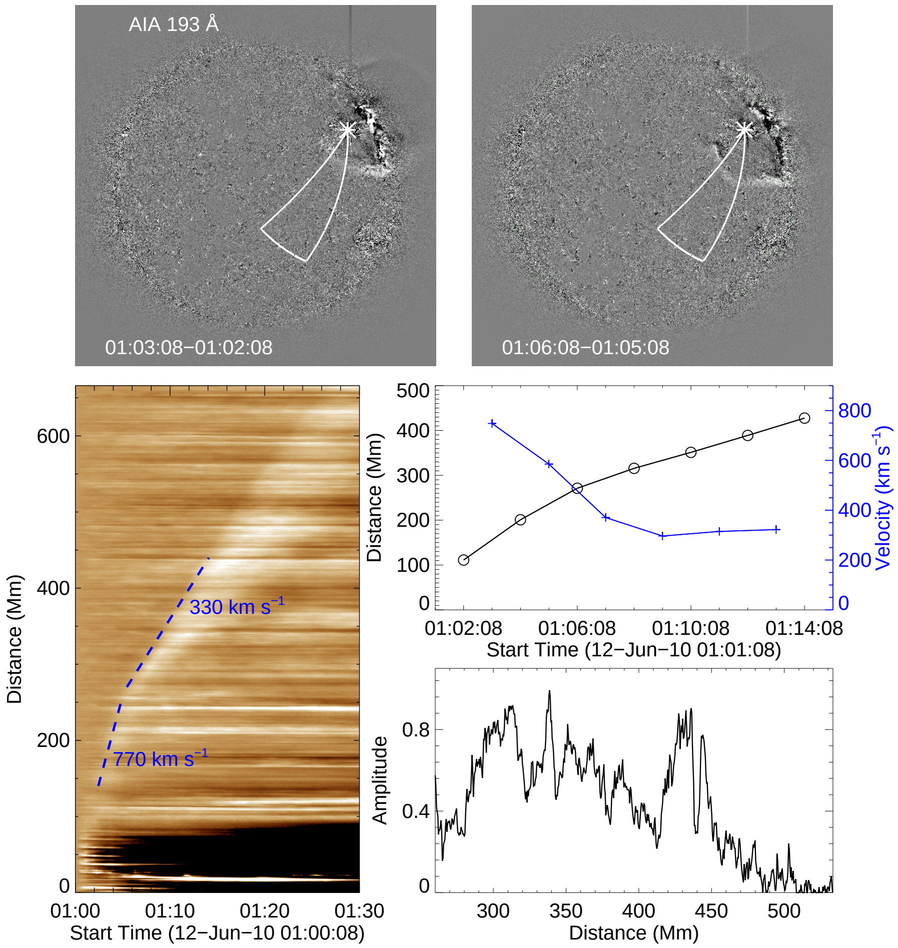

Fig. 5 *Top*: running difference images of the global coronal wave on 2010 June 12 observed by SDO/AIA. The white curves outline the 30° sector in which the perturbation profiles are calculated, starting from the determined wave center (indicated by the asterisk signs). *Bottom left*: the base ratio stack plot obtained from 12 s images over the 30° sector in the top panels. Bottom right: distance-time, velocity-time and amplitude-distance plots of the wave obtained from the base difference profiles.

et al. 2009), while others found that the constant velocity result is in fact not consistent with observations. Warmuth et al. (2001) found a deceleration of the disturbances by studying two events observed in SOHO/EIT 195 Å and Hα images. Similarly, Vršnak et al. (2002) found that the observed He I (10830 Å) and the Hα disturbances show a deceleration on the order of $100-1000$ m s^{-2}, which is comparable to the value of deceleration rate in our study (from -930 to -150 m s^{-2}).

Our results show that the velocities of the four waves vary with time, which is consistent with the result of Yang & Chen (2010). They found that the wave velocity and the local magnetic field in the corona showed significant negative correlation in most wave fronts, which can be explained by the field line stretching model. Recently, Zhukov et al. (2009) analyzed the coronal wave on 2007 December 8 and also found that the wave velocity changed a lot.

For the wave on 2010 June 12, we use the methods of fitting the leading edge of the fronts and extracting the position of maximum intensity to obtain the wave velocity. By comparing the results obtained with the two methods, we find that the velocity obtained by extracting the position of maximum intensity is smaller than that obtained by fitting the leading edge of the fronts, with an approximate difference of 20 km s^{-1}.

The velocity of the wave on 2010 June 12 shows an obvious deceleration during the propagation process. However, there are several alternative interpretations for this. The faster front before 01:05 UT might be a separate front, which is the coronal counterpart of Morton waves, as illustrated by Chen & Wu (2011). This early phase of high velocity could also be related to the fast 1 000–2 000 km s^{-1} waves found by Liu et al. (2010, see their fig. 3b) and Liu et al. (2011), which are located in the erupting AR and are somewhat different from the global EUV wave. This could explain the change of velocity in Figure 5 because this may suggest a change of dominance by the fast wave at short distance to that by the global EUV wave at large distance. Another possibility is due to the projection effects. We assume all the wave signals are on the solar surface using sector projection, but in reality there is vertical expansion of the CME or EUV wave front, which may result in a higher apparent velocity early on when the wave is close to the solar limb where line-of-sight projection is more inclined to the solar surface. The third possibility might indicate that this global wave is a real fast-mode wave, since such a feature is expected by the fast-mode wave model.

Acknowledgements We acknowledge the SECCHI consortia for providing the data. This work is supported by the National Natural Science Foundation of China (Grant Nos. 40890161, 11025315, 10921303 and 11003026), the CAS Project KJCX2-YW-T04, the National Basic Research Program of China (Grant 2011CB811403), and the Young Researcher Grant of the National Astronomical Observatories, Chinese Academy of Sciences.

References

Attrill, G. D. R. 2010, ApJ, 718, 494
Attrill, G. D. R., Harra, L. K., van Driel-Gesztelyi, L., & Démoulin, P. 2007a, ApJ, 656, L101
Attrill, G. D. R., Harra, L. K., van Driel-Gesztelyi, L., Démoulin, P., & Wülser, J.-P. 2007b, Astronomische Nachrichten, 328, 760
Biesecker, D. A., Myers, D. C., Thompson, B. J., Hammer, D. M., & Vourlidas, A. 2002, ApJ, 569, 1009
Chen, A.-Q., & Zong, W.-G. 2009, RAA (Research in Astronomy and Astrophysics), 9, 470
Chen, P. F. 2006, ApJ, 641, L153
Chen, P. F. 2008, Journal of Astrophysics and Astronomy, 29, 179
Chen, P. F. 2009, ApJ, 698, L112
Chen, P. F., Fang, C., & Shibata, K. 2005, ApJ, 622, 1202
Chen, P. F., Wu, S. T., Shibata, K., & Fang, C. 2002, ApJ, 572, L99
Chen, P. F., & Wu, Y. 2011, ApJ, 732, L20
Cliver, E. W., Laurenza, M., Storini, M., & Thompson, B. J. 2005, ApJ, 631, 604
Cohen, O., Attrill, G. D. R., Manchester, W. B., IV, & Wills-Davey, M. J. 2009, ApJ, 705, 587
Delaboudinière, J.-P., Artzner, G. E., Brunaud, J., et al. 1995, Sol. Phys., 162, 291
Delannée, C. 2000, ApJ, 545, 512
Gallagher, P. T., & Long, D. M. 2011, Space Sci. Rev., 158, 365
Gopalswamy, N., Yashiro, S., Temmer, M., et al. 2009, ApJ, 691, L123
Howard, R. A., Moses, J. D., Vourlidas, A., et al. 2008, Space Sci. Rev., 136, 67
Kaiser, M. L., Kucera, T. A., Davila, J. M., et al. 2008, Space Sci. Rev., 136, 5
Kienreich, I. W., Temmer, M., & Veronig, A. M. 2009, ApJ, 703, L118
Klassen, A., Aurass, H., Mann, G., & Thompson, B. J. 2000, A&AS, 141, 357
Lemen, J. R., Title, A. M., Akin, D. J., et al. 2011, Sol. Phys., 172

Li, T., Zhang, J., Zhang, Y., & Yang, S. 2011, ApJ, 739, 43
Li, T., Zhang, J., Zhao, H., & Yang, S. 2010, ApJ, 720, 144
Liu, W., Nitta, N. V., Schrijver, C. J., Title, A. M., & Tarbell, T. D. 2010, ApJ, 723, L53
Liu, W., Title, A. M., Zhao, J., et al. 2011, ApJ, 736, L13
Long, D. M., Gallagher, P. T., McAteer, R. T. J., & Bloomfield, D. S. 2008, ApJ, 680, L81
Ma, S., Wills-Davey, M. J., Lin, J., et al. 2009, ApJ, 707, 503
Moreton, G. E., & Ramsey, H. E. 1960, PASP, 72, 357
Muhr, N., Veronig, A. M., Kienreich, I. W., Temmer, M., & Vrsnak, B. 2011, arXiv: 1107.0921
Patsourakos, S., & Vourlidas, A. 2009, ApJ, 700, L182
Patsourakos, S., Vourlidas, A., Wang, Y. M., Stenborg, G., & Thernisien, A. 2009, Sol. Phys., 259, 49
Podladchikova, O., & Berghmans, D. 2005, Sol. Phys., 228, 265
Schwer, K., Lilly, R. B., Thompson, B. J., & Brewer, D. A. 2002, AGU Fall Meeting Abstracts, C1
Smith, S. F., & Harvey, K. L. 1971, in Astrophysics and Space Science Library, Physics of the Solar Corona, ed. C. J. Macris, 27, 156
Thompson, B. J., & Myers, D. C. 2009, ApJS, 183, 225
Thompson, B. J., Plunkett, S. P., Gurman, J. B., et al. 1998, Geophys. Res. Lett., 25, 2465
Uchida, Y. 1968, Sol. Phys., 4, 30
Veronig, A. M., Muhr, N., Kienreich, I. W., Temmer, M., & Vršnak, B. 2010, ApJ, 716, L57
Veronig, A. M., Temmer, M., & Vršnak, B. 2008, ApJ, 681, L113
Vršnak, B., & Cliver, E. W. 2008, Sol. Phys., 253, 215
Vršnak, B., Warmuth, A., Brajša, R., & Hanslmeier, A. 2002, A&A, 394, 299
Wang, Y.-M. 2000, ApJ, 543, L89
Warmuth, A., Vršnak, B., Aurass, H., & Hanslmeier, A. 2001, ApJ, 560, L105
Warmuth, A., Vršnak, B., Magdalenić, J., Hanslmeier, A., & Otruba, W. 2004, A&A, 418, 1117
Wills-Davey, M. J. 2006, ApJ, 645, 757
Wills-Davey, M. J., & Attrill, G. D. R. 2009, Space Sci. Rev., 149, 325
Wills-Davey, M. J., DeForest, C. E., & Stenflo, J. O. 2007, ApJ, 664, 556
Wuelser, J.-P., Lemen, J. R., Tarbell, T. D., et al. 2004, in Society of Photo-Optical Instrumentation Engineers (SPIE) Conference Series 5171, eds. S. Fineschi, & M. A. Gummin, 111
Yang, H. Q., & Chen, P. F. 2010, Sol. Phys., 266, 59
Zhukov, A. N., & Auchère, F. 2004, A&A, 427, 705
Zhukov, A. N., Rodriguez, L., & de Patoul, J. 2009, Sol. Phys., 259, 73